Synthesis, characterization, single crystal X-ray and DFT analysis of disubstituted phosphorodithioates

Article *in* Journal of Molecular Structure · April 2018

DOI: 10.1016/j.molstruc.2017.12.103

CITATION
1

READS
251

8 authors, including:

Mandeep Kour
University of Jammu
10 PUBLICATIONS **8** CITATIONS
SEE PROFILE

Dr. Sandeep Kumar
University of Jammu
26 PUBLICATIONS **49** CITATIONS
SEE PROFILE

Ahmed Feddag
Université Abdelhamid Ibn Badis Mostaganem
2 PUBLICATIONS **2** CITATIONS
SEE PROFILE

Abdelkader Chouaih
Université Abdelhamid Ibn Badis Mostaganem
75 PUBLICATIONS **84** CITATIONS
SEE PROFILE

Journal of Molecular Structure 1157 (2018) 708–715

Contents lists available at ScienceDirect

Journal of Molecular Structure

journal homepage: http://www.elsevier.com/locate/molstruc

Synthesis, characterization, single crystal X-ray and DFT analysis of disubstituted phosphorodithioates

Mandeep Kour [a], Sandeep Kumar [a], Ahmed Feddag [b], Savit Andotra [a], Abdelkader Chouaih [b], Vivek K. Gupta [c], Rajni Kant [c], Sushil K. Pandey [a, *]

[a] Department of Chemistry, University of Jammu, Jammu, 180006, India
[b] Laboratory of Technology and Solid Properties (LTPS), Abdelhamid Ibn Badis University, BP 227, Mostaganem, 27000, Algeria
[c] X-ray Crystallographic Laboratory, Department of Physics and Electronics, University of Jammu, Jammu, 180006, India

ARTICLE INFO

Article history:
Received 21 October 2017
Received in revised form
29 December 2017
Accepted 31 December 2017
Available online 3 January 2018

Keywords:
Dithiophosphate
Phosphorus
Sulfur
HOMO-LUMO

ABSTRACT

Disubstituted phosphorodithioates of the type $[\{(2,5\text{-}CH_3)_2C_6H_3O\}_2PS_2HNEt_3]$ (**1**) and $[\{(3,5\text{-}CH_3)_2C_6H_3O)_2(PS_2)\}_2]$ (**2**) were synthesized and characterized by IR and NMR (^1H,^{13}C and ^{31}P) spectroscopic studies and as single crystal X-ray analysis. The compound **1** crystallizes in monoclinic space group $P2_1/c$ whereas compound **2** crystallizes in triclinic space group $P\bar{1}$. The X-ray analysis reveals that in compound **1** phosphorus atom is coordinated to the two S and two O atoms to form tetrahedral geometry. The structure is stabilized by cation–anion N–H···S hydrogen bonded interactions. In compound **2**, the two phosphorus atoms have a distorted tetrahedral geometry coordinated to two $(3,5\text{-}CH_3)_2C_6H_3O$ groups. The molecule possesses a crystallographic center of symmetry and consists of *zig-zag* array of S=P–S–S–P=S linkages with two diphenyldithiophosphate moieties in the *trans* configuration. Molecular geometries, HOMO-LUMO analysis and molecular electrostatic potential of compounds **1** and **2** are investigated by theoretical calculations using B3LYP functional with the 6-311G basis combination set in the ground state and compared with the experimental values.

1. Introduction

Phosphorus-sulfur bonds within the dithiophosphato derivatives of transition metals have been shown to be strongly influenced by their extensive applications for the vulcanization of rubber [1], corrosion inhibitor [2] and analytical reagents [3]. Such novel ditolyldithiophosphate ligands appear to be potential chelating ligands to the metals, metalloids and non-metals akin to the dialkyl- and alkylene dithiophosphate ligands. Different modes of coordination shown by such soft donor ligands and are known to exist both chelating bidentate [4,5] and less common monodentate linkage [6,7]. In our laboratory, we were successful in isolating a number of triethylammonium salt of disubstituted diphenyldithiophosphates [8].

Structural studies by X-ray diffraction of several organothiophosphoryl disulfide have been reported, including $[(p\text{-}MeC_6H_4O)_2PS_2]_2$ [9], $[(i\text{-}C_3H_7O)_2PS_2]_2$ [10], $[Ph_2PS_2]_2$, $[(PhO)_2PS_2]_2$ [11] and $[OCMe_2CMe_2OPS_2]_2$ [12]. The reactive functional moiety –S–S– determines the chemical properties of these thermally stable disulfides and their photolytic properties are important in photochemically activated reactions. These disulfide were recommended for practical uses such as antioxidant and antiwear additives in ashless and extreme-pressure engine lubricant oils and are involved in the mechanism of antioxidant action of metal dithiophosphate lubricant oil additives, as stabilizers for polymer compositions and as vulcanization accelerators. Some disulfides also show fungicidal activity due to the significance of the disulfide bond in natural products [13]. However, there is no report available on the X-ray structure and theoretical calculations of disulfide of 3,5-dimethyldiphenyl dithiophosphate. The present work demonstrates the crystal structures and DFT analyses of disubstituted phosphorodithioates of 3,5-dimethyl diphenyldithiophosphate and former reported triethylammonium salt of 2,5-dimethyl diphenyldithiophosphate.

* Corresponding author.
E-mail address: kpsushil@rediffmail.com (S.K. Pandey).

https://doi.org/10.1016/j.molstruc.2017.12.103
0022-2860/

2. Experimental

2.1. Materials and instrumentation

All chemicals and solvents used in this study were of high purity. Solvents were distilled and dried using standard methods before use. Chloroform (Thomas Baker, b.p. 61 °C) was dried over P_2O_5. All the disubstitued phenols were procured from Sigma Aldrich and used without puriFIcation. Moisture was carefully excluded for the synthesis of compounds throughout the experimental manipulations by using standard Schlenk techniques. Elemental analyses (C, H, N, S) were conducted using the Elemental Analyser Vario EL-III (Indian Institute of Integrative Medicine, Jammu). Infrared spectra were recorded in the range of 4000–340 cm^{-1} on a Shimadzu FT-IR spectrophotometer (Department of Chemistry, University of Jammu, Jammu). The ^{1}H and ^{13}C NMR spectra were recorded in $CDCl_3$ using TMS as internal reference. The ^{31}P NMR spectra were recorded in $CDCl_3$ using H_3PO_4 (85%) as external reference on a Bruker Avance III 400 MHz (Department of Chemistry, University of Jammu, Jammu). All chemical shifts are reported in δ units downfield from TMS *i.e.* δ 0 ppm.

2.2. Crystallography data collection, refinement and computational details

Crystallization of compounds **1** and **2** was executed by very slow evaporation of their saturated solution in chloroform/*n*-hexane mixture (3:1) at room temperature which yielded suitable single crystals for X-ray analysis. X-ray data of compound **1** were collected on an X'calibur-Oxford Diffraction single crystal diffractometer with CCD area-detector (graphite-monochromator, Mo-Kα radiations, $\lambda = 0.71073$ Å). Data were corrected for Lorentz, polarization and absorption factors. The structure was solved by direct methods using SHELXS97 [14]. All non-H atoms were located in the best E-map. Full-matrix least-squares refinement was carried out using SHELXL97 [14]. The geometry of the molecule was calculated using WinGX [15], PARST [16] and PLATON [16]. Atomic scattering factors were taken from the International Tables for X-ray Crystallography (1992, Vol. C, Tables 4.2.6.8 and 6.1.1.4).

X-ray data of compound **2** were collected on a Bruker's Apex-II CCD diffractometer using Mo Kα ($\lambda = 0.71069$ Å) at room temperature. The data were processed by SAINT correcting for Lorentz and polarization effects. An empirical absorption correction was applied using SADABS [17]. The solution was obtained by direct methods, using SIR-92 [18] and refined by full−matrix least squares refinement methods [14] based on F^2, using SHELX-97. All non−hydrogen atoms were refined anisotropically. All calculations were performed using Wingx package [19]. Molecular drawings were obtained using DIAMOND. Version 2.1 [20]. Crystallographic data, details of the data collection, structure solution and refinements are listed in Table 1.

All the DFT calculations were performed using the Gaussian 09 [21] and the Gauss view 5.08 [22] programs. The geometrical parameters in the ground state (in gas phase) were computed using the B3LYP functional in combination with 6-311G(d,p) basis set [23–25]. The vibrational frequencies were computed in order to ensure that the optimized geometries correspond to a global minimum energy structures of the two compounds. The electronic properties, such as HOMO-LUMO, Mulliken charge populations and molecular electrostatic potential have been calculated using the same levels of theory.

2.3. Synthesis of compounds ***1–2***

2.3.1. *[{(2,5-CH_3)$_2$$C_6H_3O$}$_2$$PS_2HNEt_3$] (**1**)*

Compound **1** was synthesized by using 2,5-dimethylphenol (4.39 g, 35.93 mmol) as white crystalline solid according to the literature reported [8]. Yield: 96% (7.52 g); m.p. 62–64 °C; Anal. Calcd for $C_{16}H_{18}O_2PS_2HNEt_3$ (M.W. 439.61): C, 60.11; H, 7.80; S, 14.59, N, 3.19%. Found: C, 60.08; H, 7.75; S, 14.55; N, 3.14%. IR (KBr): 3413 b [N–H], 1150 s [ν(P)–O–C], 877 s [νP–O–(C)], 688 s [νP=S], 575 m [νP–S] cm^{-1}. ^{1}H NMR ($CDCl_3$, ppm): 1.25 (t, $J = 14.4$ Hz, 9H, CH_3 of Et_3N), 2.17 (s, 6H, 2–CH_3), 2.22 (s, 6H, 5-CH_3), 3.12 (q, 6H, CH_2 of Et_3N), 6.77 (d, $J = 7.6$ Hz, 2H, H_3), 7.02 (d, $J = 7.6$ Hz, 2H, H_4), 7.41 (s, 2H, H_6), 9.03 (s, 1H, –NH); ^{13}C NMR ($CDCl_3$, ppm): 8.53 (CH_3 of Et_3N), 16.63 (2–CH_3),20.90 (5-CH_3), 46.28 (CH_2 of Et_3N), 121.46

Table 1
Summary of the crystal structure, data collection and structure refinement parameters for compounds **1** and **2**[a].

Compound	1	2
Chemical formula	$C_{16}H_{18}O_2PS_2 \cdot C_6H_{16}N$	$C_{32}H_{36}O_4P_2S_4$
M_r	439.59	674.83
Crystal system, space group	Monoclinic $P2_1/c$	Triclinic, $P\bar{1}$
Temperature (K)	293	296
a, b, c (Å)	7.8463 (4), 16.6316 (8), 20.3943 (14)	10.2722 (7), 11.1236 (8), 17.8011 (8)
β (°)	112.627 (2)	80.627 (5), 77.259 (5), 63.473 (7)
V (Å^3)	2456.5 (3)	1770.2 (2)
Z	4	2
μ (mm^{-1})	0.30	0.39
Crystal size (mm)	0.30 × 0.20 × 0.20	0.13 × 0.10 × 0.08
Diffractometer	Xcalibur, Sapphire3 diffractometer	Bruker *APEX*-II CCD diffractometer
Absorption correction	Multi-scan	Multi-scan
T_{min}, T_{max}	0.929, 1.000	0.608, 0.745
No. of measured, independent and observed [$I > 2\sigma(I)$] reflections	6532, 4291, 3006	14601, 8020, 4430
R_{int}	0.022	0.038
$(\sin\theta/\lambda)_{max}$ (Å^{-1})	0.617	0.683
$R[F^2 > 2\sigma(F^2)]$, $wR(F^2)$, S	0.051, 0.128, 1.04	0.052, 0.122, 0.95
No. of reflections	4291	8020
No. of parameters	287	387
$(\Delta/\sigma)_{max}$	0.209	0.019
$\Delta\rho_{max}$, $\Delta\rho_{min}$ (e Å^{-3})	0.25, −0.30	0.32, −0.33

[a] Experiments were carried out with Mo Kα radiation. Refinement was with 0 restraints. Computer programs: CrysAlis PRO (Oxford Diffraction, 2010), Bruker APEX2, Bruker SAINT, SHELXS97 (Sheldrick, 2008), SHELXS97 (Sheldrick, 2008), SHELXL97 (Sheldrick, 2008), SHELXL2014 (Sheldrick, 2014), ORTEP-3 (Farrugia, 2012), Bruker SHELXTL, PLATON (Spek, 2009).

(C_6), 126.64 (C_4), 127.32(C_2), 131.11 (C_3), 136.83 (C_5), 131.11 (C_1–O); ^{31}P NMR ($CDCl_3$, ppm): 106.40 (s).

2.3.2. [{(3,5-CH_3)$_2$$C_6H_3O$)$_2$($PS_2$)}$_2$] (**2**)

[{(3,5-CH_3)$_2$$C_6H_3O$)$_2$$PS_2$}Na] was prepared by using literature method [8]. The compound **2** of the formula [{(3,5-CH_3)$_2$$C_6H_3O$)$_2$($PS_2$)}$_2$] was synthesized by the oxidation of [{(3,5-CH_3)$_2$$C_6H_3O$)$_2$$PS_2$}Na], (5.68 g, 15.76 mmol) with iodine (1.00 g, 7.88 mmol) in chloroform under inert and anhydrous conditions resulted in the formation of [{(3,5-CH_3)$_2$$C_6H_3O$)$_2$($PS_2$)}$_2$] as yellow crystalline compound. Yield: 97% (7.60 g); IR (KBr): 1159 s [ν(P)–O–C], 846 s [νP–O–(C)], 670 s [νP=S], 556 m [νP–S], 510 s [νS–S] cm^{-1}. ^{1}H NMR ($CDCl_3$, ppm): 2.29 (s, 24H, 3,5–(CH_3)$_2$), 6.54 (s, 8H, $H_{2,6}$), 6.73 (s, 4H, H_4); ^{13}C NMR ($CDCl_3$, ppm): 23.12 (3,5–(CH_3)$_2$), 122.56 ($C_{2,6}$), 128.64 (C_4), 142.33($C_{3,5}$), 154.53 (C_1–O); ^{31}P NMR ($CDCl_3$, ppm): 78.74 (s).

3. Results and discussion

[{(2,5-CH_3)$_2$$C_6H_3O$}$_2$$PS_2$$HNEt_3$] (**1**) was isolated as white crystalline solid in quantitative yield according to the literature report [8]. (Scheme 1).

[{(3,5-CH_3)$_2$$C_6H_3O$)$_2$($PS_2$)}$_2$] (**2**) was synthesized by the oxidation of the sodium salt of 3,5-dimethyl diphenyldithiophosphate with iodine in chloroform as yellow crystalline (Scheme 2). The pure disulfide was obtained after the isolation of sodium iodide thus formed during the course of reaction. The disulfide is soluble in common organic solvents *viz* benzene, toluene, chloroform, acetone, dichloromethane etc., but are insoluble in *n*-hexane and carbon tetrachloride.

3.1. IR spectra

IR spectrum of compound **1** has a broad absorption band for [νN–H] at 3413 cm^{-1}. IR absorption spectra, of compound **1** and **2** have shown two strong intensity bands in the regions 1111–1026 cm^{-1} and 960–864 cm^{-1} for [ν(P)–O–C] and [νP–O–(C)] vibrations respectively, whereas the bands for [νP-S]$_{asym}$ and [νP-S]$_{sym}$ of the diphenyldithiophosphate moiety were observed in the regions 750–677 and 580–530 cm^{-1}, respectively [8]. The appearance of a new band for [νS–S] in the region 510 cm^{-1} in the spectrum of compound **2** is also signifying of the formation of a sulfur-sulfur bond of the two dithio moiety [26].

3.2. ^{1}HNMR

In the ^{1}H NMR spectra of the compounds (**1**–**2**) show the characteristic proton resonances of the corresponding substituted phenyl protons. The splitting patterns of the peaks in the spectra of the complexes were found to be consistent with the structures. The chemical shift of the methyl (–CH_3) protons of the phenyl rings was observed as a singlet in the region 2.17–2.29 ppm. The peaks for aromatic protons of the phenyl group were observed in the region 6.54–7.41 ppm with their characteristic splitting patterns. The chemical shift of CH_3 and CH_2 protons due to Et_3N were observed at 1.25 and 3.12 ppm, respectively. Three resonances were observed for the phenyl protons in compound (**1**), whereas compound (**2**) exhibited two resonances for the phenyl protons (Scheme 3).

3.3. ^{13}C NMR

The ^{13}C NMR spectra ($CDCl_3$) of compounds (**1**–**2**) showed the chemical shifts for the methyl (–CH_3) carbons attached to the phenyl rings were found in the region 16.63–23.12 ppm. The carbon nuclei of the aryl groups displayed their resonances in the

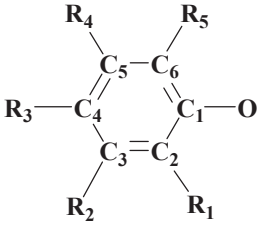

1. $\mathbf{R_1, R_4} = CH_3$, $\mathbf{R_2} = H_3$, $\mathbf{R_3} = H_4$, $\mathbf{R_5} = H_6$

2. $\mathbf{R_1} = H_2$, $\mathbf{R_2, R_4} = CH_3$, $\mathbf{R_3} = H_4$, $\mathbf{R_5} = H_6$

Scheme 3. Ring labelling for NMR spectroscopic assignments of compounds **1** and **2**.

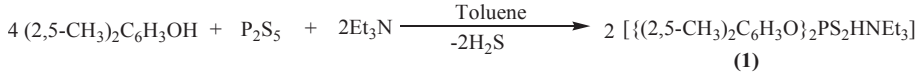

Scheme 1. Preparation of [{(2,5-CH_3)$_2$$C_6H_3O$}$_2$$PS_2$$HNEt_3$](**1**).

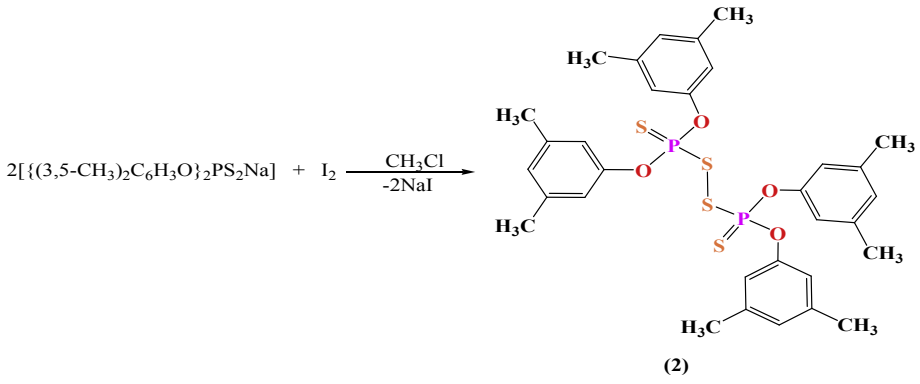

Scheme 2. Preparation of [{(3,5-CH_3)$_2$$C_6H_3O$)$_2$($PS_2$)}$_2$](**2**).

region 121.36–131.11 ppm. The chemical shift for C–O carbon nuclei was found in the region 131.11–154.53 ppm. The chemical shifts for the C–(CH_3) carbon nuclei were observed in the region 127.32–142.33 ppm.

3.4. ^{31}P NMR

The ^{31}P NMR ($CDCl_3$) spectra of the compounds (**1**–**2**) (proton-decoupled) displayed a single resonance in each case. The chemical shift of phosphorus atoms for the compounds **1** and **2** was found as a singlet at 106.40 and 78.74 ppm, respectively [27]. The occurrence of singlet for two phosphorus atoms in compound **2** is due to the chemically equivalent nature of both the phosphorus atoms of each halfmers. Further the apperance of a singlet is also justifying the purity of the compounds.

3.5. Crystal and molecular structures of compounds 1 and 2

The compounds **1** and **2** were crystallized in the monoclinic space group $P2_1/c$ and triclinic space group $P\bar{1}$, respectively. Selected bond distances and bond angles for the compounds **1** and **2** are listed in Tables 2 and 3. The optimized geometrical parameters (bond lengths and angles) for the two compounds have been calculated using the density functional theory (DFT/B3LYP/6-311G) method. The experimental structural parameters obtained from X-ray crystal structures are compared with those of optimized geometries.

A distorted tetrahedral environment around phosphorus can be clearly seen with two sulfurs and two oxygens bonded to phosphorus (Fig. 1). The compound **1** consists of triethylammonium and dithiophosphate moiety which is connected through N–H···S (Table 4) intermolecular hydrogen bond. The N–S bond distance for compound **1** is 3.313(4) Å (3.159 Å with DFT) is in close proximity with the reported value *i.e.* (3.248(6) Å) [28] for

Table 2
Selected bonds lengths (Å) and angles (°) for compound **1**.

Parameters	X-ray	DFT	Parameters	X-ray	DFT
P1–O2	1.624 (2)	1.732	P1–S2	1.9461 (11)	2.147
P1–O1	1.6115 (18)	1.778	N1–H1	0.9651	1.063
P1–S1	1.9667 (11)	2.122			
O2–P1–O1	96.23 (10)	95.02	O2–P1–S2	110.95 (9)	111.56
O2–P1–S1	110.24 (9)	113.54	O1–P1–S2	112.98 (8)	109.80
O1–P1–S1	104.89 (8)	104.94	S1–P1–S2	119.06 (5)	119.17

Table 3
Selected bonds lengths (Å) and angles (°) for compound **2**.

Parameters	X-ray	DFT	Parameters	X-ray	DFT
P1–O1	1.578 (2)	1.735	P2–O4	1.5811 (19)	1.747
P1–O2	1.5811 (18)	1.731	P2–S4	1.8902 (12)	2.058
P1–S1	1.8996 (11)	2.065	P2–S3	2.1061 (10)	2.345
P1–S2	2.0758 (12)	2.322	S2–S3	2.0549 (11)	2.225
P2–O3	1.5785 (18)	1.718			
O1–P1–O2	94.79 (11)	92.32	O3–P2–S3	107.59 (8)	106.26
O1–P1–S1	120.02 (8)	120.34	O4–P2–S3	98.12 (8)	95.93
O2–P1–S1	119.07 (9)	119.27	S4–P2–S3	115.85 (5)	119.66
O1–P1–S2	107.90 (9)	106.31	C25–O1–P1	122.57 (17)	124.64
O2–P1–S2	109.33 (9)	105.92	C1–O2–P1	123.72 (18)	124.19
S1–P1–S2	105.12 (5)	110.49	C9–O3–P2	124.31 (16)	125.55
O3–P2–O4	100.32 (10)	98.62	C17–O4–P2	125.66 (17)	124.55
O3–P2–S4	112.42 (8)	113.53	S3–S2–P1	105.76 (5)	107.70
O4–P2–S4	120.47 (9)	119.56	S2–S3–P2	103.77 (5)	105.02
O1–P1–S2–S3	40.58 (8)	39.97	O3–P2–S3–S2	−98.68 (9)	−102.09
O2–P1–S2–S3	−61.32 (10)	−57.35	O4–P2–S3–S2	157.72 (8)	157.09
S1–P1–S2–S3	169.77 (5)	172.13	S4–P2–S3–S2	28.05 (7)	28.05
P1–S2–S3–P2	110.40 (5)	93.69			

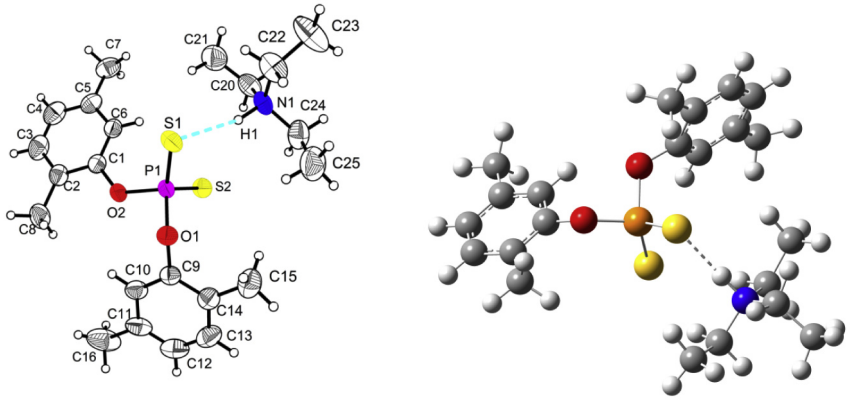

(a) **(b)**

Fig. 1. Molecular structure of [{(2,5-CH_3)$_2$$C_6H_3O$}$_2$$PS_2$$HNEt_3$] (**1**): (a) X-ray structure and (b) optimized structure.

Table 4
Selected hydrogen bonding interactions for compound **1** (The first line indicates the experimental values; the second line indicates the values obtained from the theoretical calculation).

D–H···A	H···A (Å)	D···A (Å)	D–H···A (°)
N1–H1···S1	2.391(2) 2.102	3.313(4) 3.159	159.49(20) 170.29

$[Et_3NH]^+[(OCH_2CMe_2CH_2O)PS_2]^-$. The values for the remaining hydrogen bonding parameters in compound **1** of H···S is 2.391(2) Å (2.10 Å) and N–H···S is 159.49(20)° (170° with DFT), compared to (2.44 Å and 160°) [28]. It is clear that the sulfur atom, involved hydrogen bonding, has the longer P–S bond (1.9667(11) Å) (2.0137 Å with DFT) in compound **1** whereas the sulfur atoms not involved in hydrogen bonding has shorter P–S bond length (1.9461(11) Å) (1.9864 Å with DFT). These bond lengths are longer than the terminal P=S bond observed in $HS_2POCMe_2CMe_2O$ and $HS_2POCH_2CMe_2CH_2O$ (1.923(2) and 1.908(2) Å) [29], respectively, but shorter than those of $K_2^+[(MeO)OPS_2]^-.H_2O$ (2.007(6) and 2.011(5) Å) [30] *i.e.* reflecting partial double bond character. The average P–O bond length in compound **1** is 1.6115(18) Å (1.648 Å with DFT) which is akin to those of $[Et_3NH]^+[(2\text{-}MeC_6H_4O)_2PS_2]^-$ (1.6115(18) Å) [31]. However, these bonds are slightly longer than found in the free acids $HS_2POCMe_2CMe_2O$ (1.5915(3) Å) and $HS_2POCH_2CMe_2CH_2O$ (1.5825(3) Å) [29].

The S–P–S bond angle for the compound **1** is 119.06(5)° (119.05° with DFT) is at par to those in $[Et_3NH]^+[(2\text{-}MeC_6H_4O)_2PS_2]^-$ (118.62(4)°) [31] and smaller than in $[Et_3NH]^+[CH_2\{6\text{-t-Bu-4-Me-}C_6H_4O\}_2P(S)(S)]^-$ (120.49(8)°) [28] while longer compared to the ligands like $HS_2POCMe_2CMe_2O$ (112.78(8)°), $HS_2POCH_2CMe_2CH_2O$ (115.64(8)°) [29] and $K_2^+[(MeO)OPS_2]^-.H_2O$ (113.67(3)°) [30]. The O–P–O bond angle of 96.23(10)° (96.69° with DFT) in compound (**1**) is similar to $[Et_3NH]^+[(2\text{-}MeC_6H_4O)_2PS_2]^-$ (97.07(8)°) [31] but slightly larger in the compounds $[Et_3NH]^+[CH_2\{6\text{-t-Bu-4-Me-}C_6H_4O\}_2P(S)(S)]^-$ (103.5(4)°) [28], $HS_2POCMe_2CMe_2O$ (105.1(1)°) [29], $K_2^+[(MeO)OPS_2]^-.H_2O$ (100.93(7)°) [30] and $[Et_3NH]^+[(OCH_2CMe_2CH_2O)_2PS_2]^-$(101.4(2)°) [28].

The N–H bond length in compound (**1**) is 0.9651 Å (1.06 Å with DFT), which is in reasonable agreement with the values found in [{(3,5-CH_3)$_2$$C_6H_3O$}$_2$$PS_2HNEt_3$] (0.94(4) Å) [8] (Table 3). P1–S1 and P1–S2 bond lengths for compound (**1**) are 1.9463(11) (2.013 Å with DFT) and 1.9665(11)Å (1.986 Å with DFT). These bond lengths are comparable with [{(3,5-CH_3)$_2$$C_6H_3O$}$_2$$PS_2HNEt_3$] (1.9389(12) and 1.9586(12) Å) [8].

In compound **2**, the two phosphorus atoms have a distorted tetrahedral geometry (Fig. 2) coordinated to two (3,5-CH_3)$_2$$C_6H_3O$) groups. The molecule possesses a crystallographic center of symmetry. Its backbone consists of *zig-zag* array of S=P–S–S–P=S linkages with two diphenyldithiophosphate moieties in the *trans* configuration. In compound **2**, the S–S bond length [2.0549(11) Å (2.225 Å with DFT)] is comparable to the bond length found in $[OCMe_2CMe_2OPS_2]_2$ [12] (2.058(7)Å) and $[(PhO)_2PS_2]_2$ [11] (2.070(1)Å). However, this bond length is found shorter as compared to the $[\{(i\text{-Pr})O\}_2PS_2]_2$ [10] (2.109(4)Å) and $[(p\text{-}MeC_6H_4O)_2PS_2]_2$ [9]. The P1–S2(bridge) and P1–S1(terminal) bond distances in compound **2** are 2.0758(12) (2.322 Å with DFT) and 1.8996(11)Å (2.065 Å with DFT), respectively, are comparable to values found in $[(p\text{-}MeC_6H_4O)_2PS_2]_2$ [9] (2.0693(8) and 1.9022(8)), $[\{(i\text{-Pr})O\}_2PS_2]_2$ [10] (2.072(2) and 1.908(3) Å), $[(PhO)_2PS_2]_2$ [11] (2.076(2) and 1.899(2)Å) and $[OCMe_2CMe_2OPS_2]_2$ [12] (2.082(6) and 1.908(8) Å). The P2–O3 and P2–O4 bond lengths in compound **2** are 1.5785(18) (1.718 with DFT) and 1.581(19) Å (1.747 Å with DFT) which are identical to $[(p\text{-}MeC_6H_4O)_2PS_2]_2$ [9] (1.578(2) Å), but differ in $[\{(i\text{-Pr})O\}_2PS_2]_2$ [10] (1.564(4) and 1.557(4) Å), in $[(PhO)_2PS_2]_2$ [11] (1.600(3) and 1.567(3)Å), in $[OCMe_2CMe_2OPS_2]_2$ [12] (1.54(2) and 1.59(2) Å), in [{3,4-CH_3)$_2$$C_6H_3O$}$_2$$PS_2$]$_2$Co($C_5H_5N$)$_2$

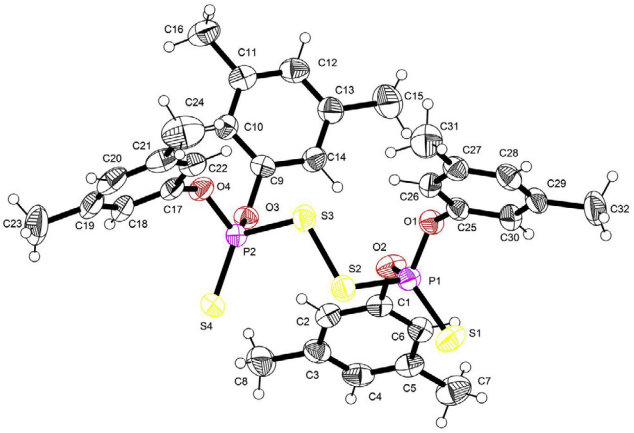

(a)

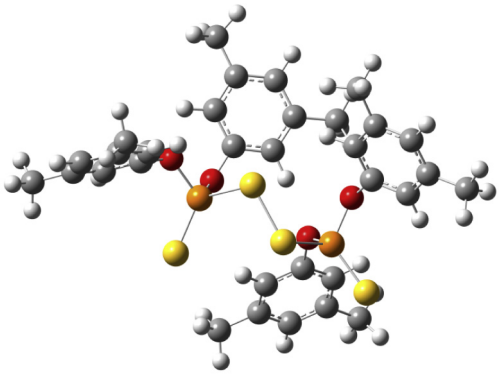

(b)

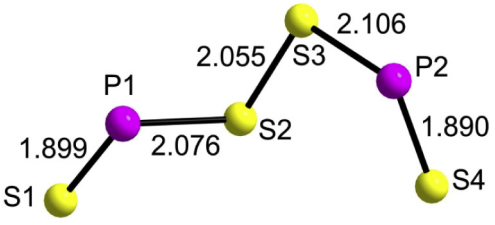

(c)

Fig. 2. Molecular structure of [{(3,5-CH_3)$_2$$C_6H_3O$)$_2$($PS_2$)}$_2$] (**2**); (**a**) X-ray structure (**b**) optimized structure and (**c**) *zig-zag* array of S=P–S–S–P=S.

(1.601(3) and 1.595(2) Å) [32] and in [{(o-$CH_3C_6H_4O)_2PS_2$}$_3$V] (1.71468 Å) [33]. All of these distances are consistent with the expected double-bond character associated with (p-d)π-bonding falling between the typical values for P–O (1.76 Å) and P=O (1.44 Å).

The S1=P1–S2 bond angle of compound **2** is 105.12(5)° (110.49° with DFT) lies between the values found in [$OCMe_2CMe_2OPS_2$]$_2$ [12] (103.3(4)°), [{(*i*-Pr)O}$_2PS_2$]$_2$ [10] (104.8(1)°) and those in [$(PhO)_2PS_2$]$_2$ [11] (107.92(8)° and 108.39(7)°), the latter being closest to the all tetrahedral angle of 109.47°. The remaining bond angles around phosphorus in compound **2** range from the smallest, O1–P1–O2 (94.79(11)°) (92.32° with DFT), to the largest, O2–P1=S1 (119.07(9)°) (119.27° with DFT) and O4–P2=S4 (120.47(9)) (119.55° with DFT) with O1–P1–S2 (107.90(9)°) (106.31° with DFT) and O2–P1–S2 (109.33(9)° (105.92° with DFT) closest to 109.47°. Identical patterns can be seen in the reported disulfides [9–12]. The S2–S3–P2 bond angles in compound **2** are similar to those in [$(PhO)_2PS_2$]$_2$ [11] (101.38(6)° and 104.26(6)°) larger than value found in [{(*i*-Pr)O}$_2PS_2$]$_2$ [10] (100.5(1)°), [(*p*-$MeC_6H_4O)_2PS_2$]$_2$ [9] (100.42(4)°) whereas smaller than those in [$OCMe_2CMe_2OPS_2$]$_2$ [12] (108.5(3)°).

The S–S–P=S units in disulfides can be described as possessing an *anti-anti* or *transoid* [11] geometry in which the S–P–S–S torsion angle tend towards 180° or, by contrast, a *syn-syn* or *cisoid* [11] geometry in which the S–P–S–S torsion angle tends towards 0°. Clearly, compound **2** has an *anti-anti* or *transoid* geometry [11] with the (3,5-$CH_3)_2C_6H_3O$) groups of the tetrahedrally coordinated phosphorus atom. A relationship between the torsion angle, the S–P–S bond angle and the P–S bond length has been indicated. The bond angle S–P–S in the compound **2** is 105.12(5)°, where the geometry is transoid, however, in [$(PhO)_2PS_2$]$_2$ [11], which has a cisoid geometry, this angle is 114.44(4)°. The opening of this S–P–S angle in the *cisoid* form is associated with a lengthening of the P–S single bond and a shortening of the S–S bond in [$(PhO)_2PS_2$]$_2$ [11] (2.139(1) and 2.0271(9)Å), respectively, compared with those in compound **2**, 2.106(10) and 2.0549(11) Å, respectively.

Finally, these results confirmed the good agreement between calculated and experimental parameters. The small differences can be due to the fact that calculated geometrical parameters are obtained in gas phase while the experimental data are acquired in the solid state [34].

3.6. Frontier molecular orbitals

Frontier molecular orbitals contain most important quantum chemical parameters such as the highest occupied molecular orbital (HOMO) and the lowest unoccupied molecular orbital (LUMO) are related to the ionization potential and the electron affinity of molecules, respectively. These two particular orbitals play a crucial role in the chemical stability of the molecules. Numerous studies are available indicating that the HOMO–LUMO gap can be used as a quantum descriptor in establishing correlation in various chemical and biochemical systems [35,36]. The frontier

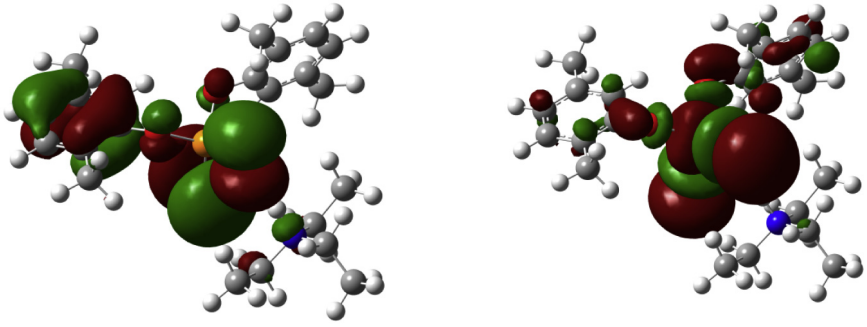

(a)

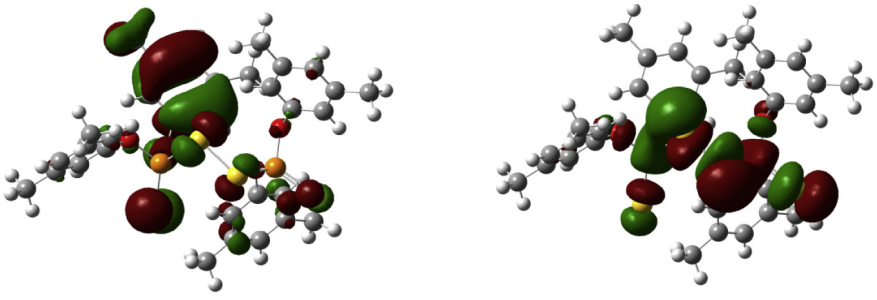

(b)

Fig. 3. HOMO and LUMO plot: (a) compound **1**, (b) compound **2**.

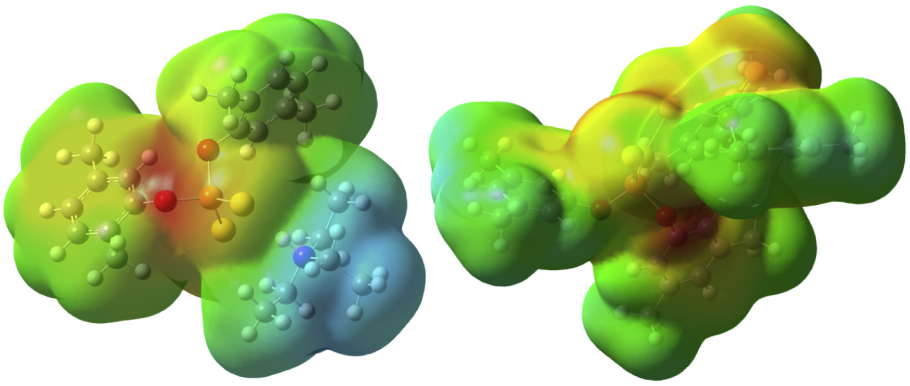

(a) (b)

Fig. 4. MEP surfaces: (a) compound **1**, (b) compound **2**.

orbital, HOMO and LUMO energies help to characterize the chemical reactivity and kinetic stability of a molecule [37,38]. The distributions of HOMO and LUMO orbitals for compounds **1** and **2** calculated at B3LYP functional with 6-311G basis set are shown in Fig. 3. For compound **1**, the HOMO orbital is delocalized over the S atoms and distributed over the conjugation plane of the C1 – C6 ring. Whereas, the LUMO orbital is localized on the P, S and O atoms. For compound **2**, the HOMO orbital is distributed over the conjugation plane of the C1 – C6 aromatic ring, while the LUMO orbital is localized on the P, S and O atoms. The band gap energies calculated at B3LYP functional with 6-311G basis set are 4.34 and 3.28 eV for compounds **1** and **2**, respectively, which indicate the molecular stability. In addition, the calculated LUMO of compound 2 showed that antibonding the LUMO is localized on the disulfide bond. Therefore, cleavage of the disulfide bond is expected upon nucleophilic attack and/or reduction.

3.7. *MEP surface*

Molecular electrostatic potential (MEP) provides a visual method to understand the reactivity of the molecules and correlates with dipole moment. Using B3LYP/6-311G optimized geometry, the MEP maps of compounds **1** and **2** are computed and their surface maps are shown in Fig. 4. Fig. 4(a) shows that for compound **1** the nucleophilic region (red) is located entirely on the oxygen and sulfur atoms, while the electrophilic region (blue) is located over the hydrogen atoms of the triethylammonium group. Fig. 4(b) indicates that for compound **2** the nucleophilic region is located mainly on O and S atoms, while the electrophilic region is located over the hydrogen atoms of all the methyl groups.

4. Conclusion

We have reported the spectroscopic, single crystal X-Ray and DFT analysis of two phosphorodithioates namely triethylammonium salt of 2,5-dimethyl diphenyldithiophosphate and disulfide of 3,5-dimethyl diphenyldithiophosphate. The optimized geometrical parameters are found in good agreement with the obtained single X-ray diffraction parameters. The X-ray analysis reveals that in triethylammonium salt of 2,5-dimethyl diphenyldithiophosphate phosphorus atom is coordinated to the two S and two O atoms to form tetrahedral geometry. The structure is stabilized by cation–anion N–H···S hydrogen bonded interactions. In disulfide of 3,5-dimethyl diphenyldithiophosphate, the two phosphorus atoms have a distorted tetrahedral geometry coordinated to two (3,5-$CH_3)_2C_6H_3O$ groups. The molecule possesses a crystallographic center of symmetry. Its backbone consists of *zig-zag* array of S=P–S–S–P=S linkages with two diphenyldithiophosphate moieties in the *trans* configuration. The HOMO-LUMO calculation allowed to obtain energy gaps for compounds **1** and **2**, which have been found to be 4.34 and 3.28 eV, respectively. According to MEP surfaces, oxygen and sulfur atoms have relatively the most negative potential, while hydrogen atoms carry the most positive potential.

Acknowledgments

The authors are grateful to the NMR laboratory Department of Chemistry, University of Jammu, Jammu for providing NMR spectral facilities (PURSE program). One of the authors (Rajni Kant) acknowledges the DST for the single crystal X-ray diffractometer as a National Facility under Project No. SR/S2/CMP-47/2003.

Appendix A. Supplementary data

CCDC 1545453 and 1545454 contain the supplementary crystallographic data for compounds **1** and **2**, respectively. These data can be obtained free of charge via http://www.ccdc.cam.ac.uk/conts/retrieving.html, or from the Cambridge Crystallographic Data Center, 12 Union Road, Cambridge CB2 1EZ, UK; fax: (+44) 1223-336-033; or e-mail: deposit@ccdc.cam.ac.uk.

References

[1] J.A. McCleverty, S. Gill, R.S.Z. Kowalski, N.A. Bailey, H. Adams, K.W. Lumbard, M.A. Murphy, J. Chem. Soc. Dalton Trans. (1982) 493–503.
[2] C. Lai, B. Xie, C. liu, W. Gou, L. Zhou, X. Su, L. Zou, Int. J. Corr. 2017 (2017) 1–2, https://doi.org/10.1155/2017/5041347.
[3] Y. Xu, J. Hazard Mater. 137 (2006) 1636–1642.
[4] R. Chander, B.L. Kalsotra, S.K. Pandey, Indian J. Chem. 43A (2004) 1134–1138.
[5] U.N. Tripathi, Phosphorus, Sulfur, Silicon Relat. Elem. 159 (2000) 47–54.
[6] P.S. Shetty, Q. Fernando, J. Am. Chem. Soc. 92 (1970) 3964–3969.
[7] K.C. Molloy, M.B. Hossain, D.V. Helon, J.J. Zuckerman, I. Haiduc, Inorg. Chem. 18 (1979) 3507–3511.
[8] R. Khajuria, S. Kumar, A. Syed, G. Kour, S. Anthal, V.K. Gupta, R. Kant, S.K. Pandey, J. Coord. Chem. 67 (2014) 2925–2941.
[9] C. Gurnani, S. Maheshwari, R. Ratnani, J.E. Drake, Anal. Sci.: X-ray Struct. Anal. Online 24 (2008) 197–198.
[10] S.L. Lawton, Inorg. Chem. 9 (1970) 2269–2274.
[11] A.C. Gallacher, A.A. Pinkerton, Acta Crystallogr. C49 (1993) 1793–1796.
[12] J.S. Yadav, R. Bohra, R.K. Mehrotra, A.K. Rai, G. Srivastava, Acta Crystallogr. C45 (1989) 308–311.
[13] I. Haiduc, L.Y. Goh, Coord. Chem. Rev. 224 (2002) 151–170.
[14] G.M. Sheldrick, Acta Crystallogr. A64 (2008) 112–122.

[15] M. Nardelli, J. Appl. Crystallogr. 28 (1995) 659.
[16] A.L. Spek, Acta Crystallogr. D65 (2009) 148–155.
[17] SADABS-2008/1-Bruker AXS area detector scaling and absorption correction.
[18] A. Altomare, G. Cascarano, C. Giacovazzo, A. Guagliardi, J. Appl. Crystallogr. 26 (1993) 343–350.
[19] L.J. Farrugia, J. Appl. Crystallogr. 32 (1999) 837–838.
[20] K. Brandenburg, DIAMOND, Crystal Impact GbR, Bonn, Germany, 1998, Version 2.1. .
[21] M.J. Frisch, G.W. Trucks, H.B. Schlegel, G.E. Scuseria, M.A. Robb, J.R. Cheeseman, J.A. Montgomery Jr., T. Vreven, K.N. Kudin, J.C. Burant, J.M. Millam, S.S. Iyengar, J. Tomasi, V. Barone, B. Mennucci, M. Cossi, G. Scalmani, N. Rega, G.A. Petersson, H. Nakatsuji, M. Hada, M. Ehara, K. Toyota, R. Fukuda, J. Hasegawa, M. Ishida, T. Nakajima, Y. Honda, O. Kitao, H. Nakai, M. Klene, X. Li, J.E. Knox, H.P. Hratchian, J.B. Cross, C. Adamo, J. Jaramillo, R. Gomperts, R.E. Stratmann, O. Yazyev, A.J. Austin, R. Cammi, C. Pomelli, J.W. Ochterski, P.Y. Ayala, K. Morokuma, G.A. Voth, P. Salvador, J.J. Dannenberg, V.G. Zakrzewski, S. Dapprich, A.D. Daniels, M.C. Strain, O. Farkas, D.K. Malick, A.D. Rabuck, K. Raghavachari, J.B. Foresman, J.V. Ortiz, Q. Cui, A.G. Baboul, S. Clifford, J. Cioslowski, B.B. Stefanov, G. Liu, A. Liashenko, P. Piskorz, I. Komaromi, R.L. Martin, D.J. Fox, T. Keith, M.A. Al-Laham, C.Y. Peng, A. Nanayakkara, M. Challacombe, P.M.W. Gill, B. Johnson, W. Chen, M.W. Wong, C. Gonzalez, J.A. Pople, Gaussian 09, Revision B01, Gaussian Inc, Pittsburgh PA, 2010.
[22] A.E. Frisch, H.P. Hratchian, R.D. Dennington, T.A. Keith, J. Millam, A.B. Nielsen, A.J. Holder, J. Hiscocks, Gauss View, Gaussian Inc., Carnegie Office Park, Building 6, Pittsburg, PA 15106, USA, 2009, Version 5.0.8. .
[23] A.D. Becke, J. Chem. Phys. 98 (1993) 5648–5652.
[24] C. Lee, W. Yang, R.G. Parr, Phys. Rev. B 37 (1988) 785–789.
[25] P.J. Stephens, F.J. Devlin, C.F. Chabalowski, M.J. Frisch, J. Phys. Chem. 98 (1994) 11623–11627.
[26] B.A. Trofimov, L.M. Sinegovskaya, N.K. Gusarova, J. Sulfur Chem. 30 (2009) 518–554.
[27] C. Glidewell, Inorg. Chim. Acta. 25 (1977) 159–163.
[28] K.C. Kumaraswamy, S. Kumaraswamy, S. Raja, K.S. Kumar, J. Chem. Crystallogr. 31 (2001) 51–56.
[29] J.E. Drake, L.N. Khasrou, A.G. Mislanker, R. Ratnani, Polyhedron 19 (2000) 407–412.
[30] M.C. Gupta, (Ph.D. Thesis), University of Rajasthan, India (2004).
[31] J.E. Drake, C.L. B Macdonald, A. Kumar, S.K. Pandey, R. Ratnani, J. Chem. Crystallogr. 35 (2005) 447–450.
[32] S. Kumar, G. Kour, G. Schreckenbach, S. Andotra, G. Hundal, V. Sharma, S. Jaglan, S.K. Pandey, J. Mol. Struct. 1141 (2017) 23–30.
[33] S. Kumar, A. Syed, S. Andotra, R. Kaur Vikas, S.K. Pandey, J. Mol. Struct. 1154 (2018) 165–178.
[34] S. Guner, Y. Atalay, A. Dolma, J. Mol. Struct. 984 (2010) 389–395.
[35] P. Thanikaivelan, V. Subramanian, J. Raghava Rao, B.U. Nair, Chem. Phys. Lett. 323 (2000) 59–70.
[36] D.F.V. Lewis, C. Ioannides, D.V. Parke, Xenobiotica 24 (1994) 401–408.
[37] I. Fleming, Frontier Orbitals and Organic Chemical Reactions, John Wiley and Sons, New York, 1976.
[38] Y. Tao, L. Han, Y. Han, Z. Liu, Spectrochim. Acta A 137 (2015) 892–898.